Assessing the Performance Gap Between Conservative Voltage Reduction Optimization and Realistic Network Simulations

Wenhao Lin
Dept. of Electrical and Electronic Engineering
The University of Manchester, Manchester M13 9PL, U.K.
wenhao.lin@postgrad.manchester.ac.uk

Firdous Ul Nazir
Dept. of Electrical and Electronic Engineering
Glasgow Caledonian University, Glasgow G4 0BA, U.K.
FirdousUl.Nazir@gcu.ac.uk

Bikash Pal
Dept. of Electrical and Electronic Engineering
Imperial College London, London SW7 2AZ, U.K.
b.pal@imperial.ac.uk

Ali Ahmadi
Ernst & Young, London, U.K.
ali.ahmadi@uk.ey.com

***Abstract*—This paper examines the performance gap between conservative voltage reduction (CVR) optimization and its implementation in unbalanced distribution networks. Using closed-loop OPF–GridLAB-D co-simulation on the IEEE 13- and 123-bus systems, we compare four OPF formulations from linear to unbalanced second-order cone programming (SOCP). Results show that higher-fidelity models reduce voltage setpoint mismatches, but residual errors remain due to inaccurate load parameters, especially constant-impedance assumptions in ZIP models. Time-varying and thermostatically controlled load behaviors further introduce systematic biases, limiting CVR benefits or causing undervoltages. The paper highlights the need for high-fidelity unbalanced modeling and adaptive load parameter estimation for reliable CVR deployment.**

***Index Terms*—Co-simulation, Conservative Voltage Reduction, Optimal Power Flow, Second-order Cone Programming, Unbalanced Distribution Networks.**

I. Introduction

The global shift toward low-carbon and smart energy systems has increased the operational complexity of power distribution networks. Among demand-side strategies, conservative voltage reduction (CVR) is a cost-effective method to reduce peak demand by operating voltages near the lower regulatory limit, as most loads are voltage dependent and consume less power under reduced voltage.

CVR is typically implemented using coordinated control of on-load tap changers (OLTCs), switched shunt capacitors (SSCs), and distributed generation (DG) inverters. Its performance is usually evaluated via simulation-based studies modeling voltage-dependent loads under varying conditions. However, many works assume that the optimal power flow (OPF) solution represents the true operating point without re-solving the nonlinear AC power flow [1]–[3]. This assumption blurs the boundary between optimization and simulation and can lead to an overestimation of CVR benefits, particularly when simplified or inaccurate load models are employed.

While these simulations offer repeatability and flexibility, particularly when field trials are impractical, many studies rely on overly simplified system and load models. Common limitations include fixed ZIP (constant impedance, current, and power) load models that ignore stochastic demand and the periodic behavior of thermostatically controlled loads (TCLs) [1]–[7]. Although CVR may temporarily reduce TCL power consumption, rebound effects can offset energy savings over time [8].

This paper develops a closed-loop OPF–GridLAB-D co-simulation framework to quantify the implementation gap of CVR, i.e., the mismatch between OPF-predicted voltages and the voltages realized after applying the computed setpoints. Unlike studies that assess CVR benefits directly from OPF solutions, we implement OPF-derived control actions in an unbalanced time-series simulator and evaluate both voltage error and CVR outcomes using simulated results as ground truth. Using this unified platform, we provide a benchmark of four OPF formulations from linear to unbalanced second-order cone programming (SOCP), and further show that tight relaxation gaps do not guarantee accurate voltage tracking when static ZIP assumptions face stochastic residential/TCL behaviors, motivating adaptive load-parameter tracking for reliable CVR deployment.

II. Problem Formulation and Model Development

In this work, the CVR objective is formulated by directly minimizing the active power drawn from the substation, P_{sub}. Since renewable power injections forecasts can be assumed to be close to their average forecasts throughout the optimisation window, P_{sub} provides a compact and physically meaningful measure of the overall power consumption of the distribution network.

$$\min P_{\text{sub}} \tag{1}$$

979-8-3315-8138-1

A. Nomenclature

For each branch (i,j), P_{ij} and Q_{ij} denote the active and reactive power flow from bus i to bus j, with line parameters r_{ij} and x_{ij}. The squared voltage magnitude and squared current magnitude are denoted by u_i and l_{ij}. At bus j, P_j^l and Q_j^l represent the net active and reactive load demand.

B. Mixed-Integer Modeling of Power Flow Control Devices

All power flow control devices are represented as mixed-integer constraints integrated into the optimization model:

$$\sum_{k=1}^{n_t} z_k^t = 1, \quad z_k^t \in \{0,1\}, \tag{2}$$

$$\sum_{k=1}^{n_t} T_{ij}^k w_k = u_j, \quad w_k = z_k^t u_j^f, \tag{3}$$

$$u_j^f - M(1-z_k^t) \le w_k \le u_j^f + M(1-z_k^t), \tag{4}$$

$$-Mz_k^t \le w_k \le Mz_k^t, \tag{5}$$

$$Q_j^{\mathrm{SSC}} = \sum_{k=1}^{n_q} z_k^q Q_{j,k}^{\mathrm{SSC}}, \quad \sum_{k=1}^{n_q} z_k^q = 1,\ z_k^q \in \{0,1\}, \tag{6}$$

$$|Q_j^d| \le P_j^d \tan\left(\cos^{-1} \underline{pf_j^{DG}}\right). \tag{7}$$

The controllable devices are modeled via mixed-integer constraints in (2)–(7). For the OLTC, (2) enforces a one-hot tap selection using binary variables z_k^t, and (3) applies the corresponding tap ratio T_{ij}^k to the voltage relationship. The bilinear term introduced by tap selection is linearized by the Big-M constraints in (4)–(5) using an auxiliary variable w_k and a sufficiently large constant M. For the SSC, (6) uses binary variables z_k^q to switch discrete capacitor steps, resulting in a reactive injection Q_j^{SSC}. Finally, (7) imposes the DG power-factor limit, restricting Q_j^d as a function of P_j^d and the minimum power factor $\underline{pf_j^{DG}}$.

C. Power Flow Relaxations

To evaluate the impact of modeling accuracy on CVR performance, four levels of power flow relaxations are considered in the OPF formulation: (1) a linear branch-flow model obtained by neglecting current-squared terms and linearizing voltage drops [9]; (2) a SOCP relaxation without mutual impedance terms; (3) a SOCP model including mutual impedance coupling under the balanced operation assumption; and (4) an unbalanced three-phase SOCP formulation that iteratively updates the coupling coefficients to account for phase asymmetry [10]. The unified SOCP formulation is expressed as

$$P_{ij} = P_j^l + \sum_{k:(j,k)\in\mathcal{E}} P_{jk} + r_{ij} l_{ij}, \tag{8}$$

$$Q_{ij} = Q_j^l + \sum_{k:(j,k)\in\mathcal{E}} Q_{jk} + x_{ij} l_{ij}, \tag{9}$$

$$u_j = u_i - 2(r_{ij}P_{ij} + x_{ij}Q_{ij}) + (r_{ij}^2 + x_{ij}^2) l_{ij}, \tag{10}$$

$$P_{ij}^2 + Q_{ij}^2 \le u_i l_{ij}. \tag{11}$$

$$u_{min} \le u_j \le u_{max} \tag{12}$$

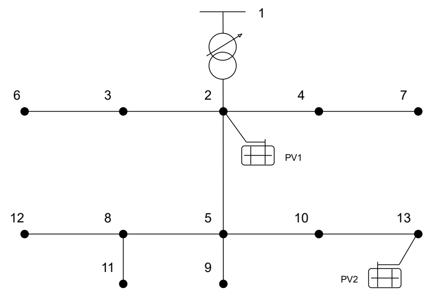

Fig. 1. The modified IEEE 13-bus feeder.

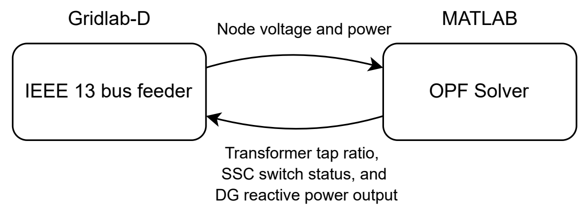

Fig. 2. Co-simulation architecture.

Equations (8) and (9) enforce active and reactive power balance along each node. Equation (10) represents the voltage drop relationship between connected nodes. Equation (11) is the second-order cone constraint, and the relaxation gap is defined as the norm of the residuals of this constraint aggregated over all branches, i.e., $\|P_{ij}^2 + Q_{ij}^2 - u_i l_{ij}\|_2$. When mutual impedance is considered, coupling terms are added to the voltage drop expression. In (12), the squared voltage magnitude is constrained to $[0.9^2, 1.1^2]$ p.u. consistent with the utilization voltage range specified in ANSI C84.1 [11]. The lower bound is intentionally set at 0.9 p.u. to accentuate the practical impact of voltage estimation errors and more clearly reveal performance differences among the OPF formulations.

III. Algorithm Deployment

A. Feeder Configuration and Residential Load Composition

The simulation setup follows the IEEE 13-bus distribution feeder as shown in Fig. 1, with static loads replaced by aggregated residential loads representing 601 households. Each household comprises typical residential appliances with stochastic parameters, such as heating type and floor area, configured consistently with the simulation setup reported in [12]. In that configuration, all building-level parameters except for heating type are sampled from uniform distributions within predefined ranges. Photovoltaic (PV) units are added to the IEEE 13-bus feeder to reach an 8% capacity penetration. PV outputs are determined by local weather conditions, and SSCs operate in a binary on/off mode.

B. Co-simulation Architecture

Co-simulation is an advanced analysis method that enables simulators from different domains to interact during runtime

979-8-3315-8138-1

by dynamically exchanging data. Hierarchical engine for large-scale infrastructure co-simulation (HELICS) is a versatile co-simulation platform designed to facilitate the integration of diverse simulators across multiple computational environments and programming languages [13]. As shown in Fig. 2, there are two federates in this paper: the IEEE 13-bus feeder and the OPF solver. The power flow simulation of the IEEE 13-bus feeder with residential loads is conducted using GridLAB-D. It accurately models the multiphase mutual coupling and unbalance effects within the distribution network. Simulations are performed with a one-minute time resolution over a one-day period. The OPF is executed every 30 minutes, and the resulting nodal voltages are regarded as the forecasted voltages $\hat{V}$. The control device setpoints obtained from the corresponding OPF are implemented in GridLAB-D, and the simulated voltages are regarded as truth value. The accuracy of the OPF is evaluated by the mean absolute percentage error (MAPE) and the mean percentage error (MPE) of all nodal voltage magnitudes, computed between the OPF-predicted voltages and the corresponding simulated voltages. The truth voltages are taken at the next time step (1 min after setpoint implementation), assuming loads are approximately unchanged within this window.

C. Nominal Load Estimation Using Static ZIP Model

In the OPF formulation, residential loads are modeled using a simplified conventional ZIP model. This approximation is obtained using the binomial approximation method (BAM) [14]. Since residential loads vary with voltage, the OPF first estimates the nominal active and reactive powers using a static ZIP model. The nominal values are derived from the sampled nodal powers P_i, Q_i and the squared voltages u_i as:

$$\hat{P}_i^{l0} = \frac{P_i}{\hat{\alpha}_P + \hat{\alpha}_Z u_i}, \hat{Q}_i^{l0} = \frac{Q_i}{\hat{\beta}_P + \hat{\beta}_Z u_i}. \tag{13}$$

Once the nominal powers are obtained, the voltage-dependent load expressions are updated as:

$$P_i(u) = \hat{P}_i^{l0}(\hat{\alpha}_P + \hat{\alpha}_Z u_i), Q_i(u) = \hat{Q}_i^{l0}(\hat{\beta}_P + \hat{\beta}_Z u_i). \tag{14}$$

The ZIP coefficients used in the OPF are set as $\alpha_P = 0.242$, $\alpha_I = 0.623$, and $\alpha_Z = 0.135$, which correspond to an aggregated residential load approximation based on experimentally measured ZIP parameters reported in [15]. The effective parameters $\hat{\alpha}$ and $\hat{\beta}$ are computed using the BAM, yielding $\hat{\alpha}_P = \hat{\beta}_P = 0.5535$ and $\hat{\alpha}_Z = \hat{\beta}_Z = 0.4465$.

IV. Case Study on the IEEE 13-Bus Feeder

A total of six test cases are evaluated, as summarized in Table I. Case 1 serves as the baseline scenario without any voltage control. Case 2 utilizes the integrated Volt/VAR control (IVVC) algorithm provided within GridLAB-D, regulating the end-of-line (EOL) nodes (6, 7, 9, 11, 12, and 13) to a voltage target of 0.9 p.u. Cases 3–6 correspond to OPF-based approaches with progressively increasing model fidelity, ranging from the linear relaxation to the unbalanced three-phase SOCP formulation.

TABLE I
Description of Test Cases.

Case	Description
1	Baseline without control devices
2	IVVC with EOL voltage target of 0.9 p.u. (Phase A)
3	Linear OPF
4	SOCP without mutual impedance
5	SOCP with mutual impedance (balanced)
6	SOCP with unbalanced network characteristics

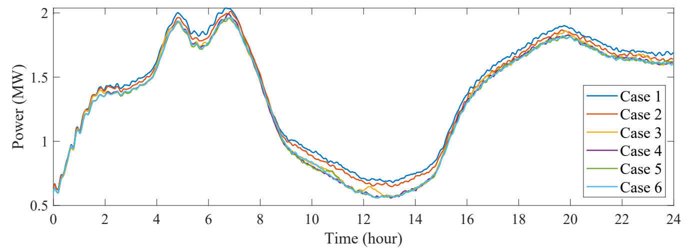

Fig. 3. Smoothed total power consumption curves for all test cases.

TABLE II
Comparison of energy, power, and MAPE under different cases.

Case	1	2	3	4	5	6
Energy (MWh)	32.799	32.407	32.276	32.293	32.220	32.168
Peak power (MW)	2.038	2.012	1.972	1.979	1.966	1.965
MAPE	–	–	1.07%	1.16%	1.12%	1.05%
Relaxation gap	–	–	–	1.4×10^{-5}	0.321	0.0763

The total power profiles of all test cases are shown in Fig. 3. Implementing CVR effectively reduces power consumption in all scenarios, with OPF-based methods achieving the greatest reduction compared to the line-compensation IVVC.

As summarized in Table II, the OPF-based CVR (Case 6) yields a substantially larger energy reduction than the IVVC baseline (0.631 MWh versus 0.392 MWh), corresponding to a relative increase in achievable energy savings. The SOCP relaxation remains exact when mutual impedance is neglected but loses exactness once coupling terms are included or the network becomes unbalanced. Although iterative refinement can reduce the relaxation gap, it cannot fully eliminate it or guarantee convergence to the exact solution.

A. Impact of Voltage Estimation Errors on CVR Optimization

The impact of OPF-computed voltage errors on CVR optimization performance is a key focus of this paper. As shown in the top panel of Fig. 4, the MAPE across all test cases remains within the range of approximately 0.4% to 1.8% over a 24-hour period. The voltage error exhibits a clear positive correlation with load magnitude. Under high-load conditions, all cases show increased voltage estimation errors. This indicates that voltage estimation accuracy is highly sensitive to load magnitude in practice, particularly during peak demand periods when load modeling inaccuracies are amplified.

As shown in the bottom panel of Fig. 4, the linear relaxation (Case 3) and the SOCP model without mutual impedance

979-8-3315-8138-1

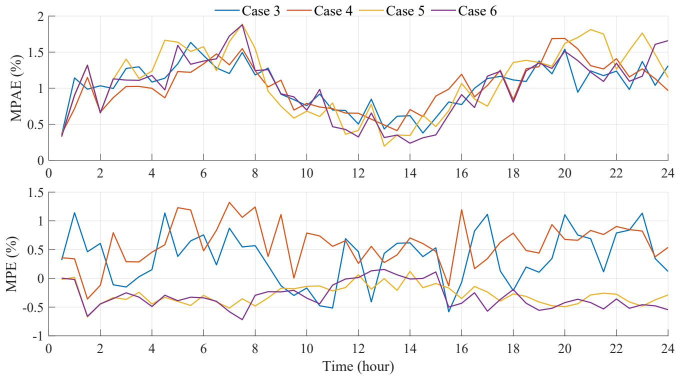

Fig. 4. Voltage error profiles for Cases 3–6: MAPE (top) and MPE (bottom).

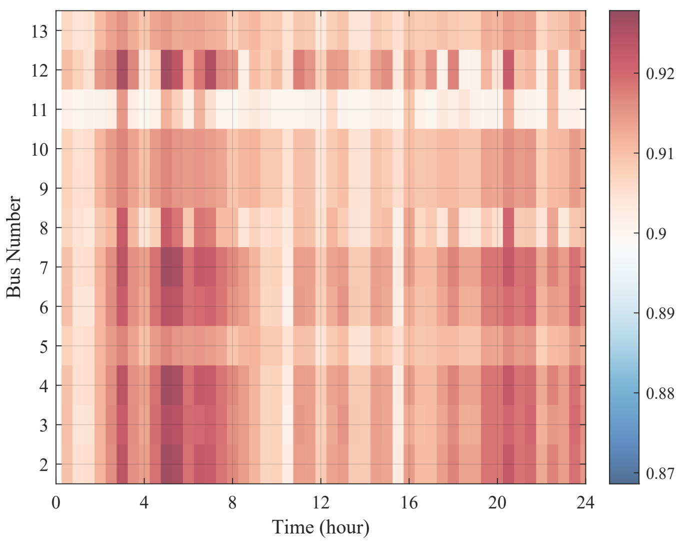

Fig. 5. OPF-predicted nodal voltage profiles on the IEEE 13 obtained from the Case 6.

(Case 4) tend to overestimate nodal voltages, limiting the degree of voltage reduction and thus the potential CVR benefits. Conversely, the SOCP formulations that account for mutual impedance (Cases 5 and 6) generally underestimate voltages, which can push some buses below the minimum voltage limit and risk operational violations.

Figs. 5 and 6 further illustrate this effect. Compared with the OPF-predicted heatmap, the simulated nodal voltage map is consistently lower across the feeder, which is consistent with the negative MPE and indicates that the OPF overestimates voltages on average. Under CVR, the optimization aims to bring the voltage at bus 11 close to 0.9 p.u.; however, after applying the OPF-derived setpoints in GridLAB-D, the voltage at bus 11 can drop to about 0.87 p.u., revealing an undervoltage outcome due to overcompensation in closed-loop implementation. In addition, the persistent overestimation at buses 5, 8, and 11 suggests that the prediction error propagates downstream and accumulates along branches, leading to increasingly pronounced deviations toward the feeder end.

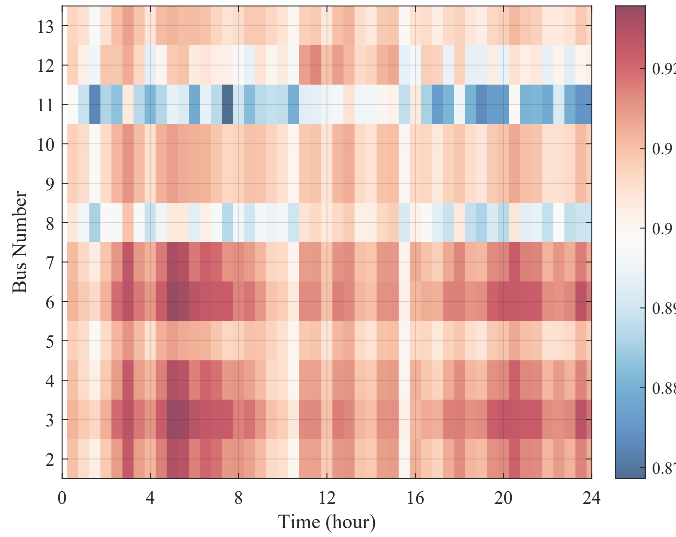

Fig. 6. Simulated nodal voltage profiles on the IEEE 13 after implementing the Case 6 OPF-derived control actions in GridLAB-D.

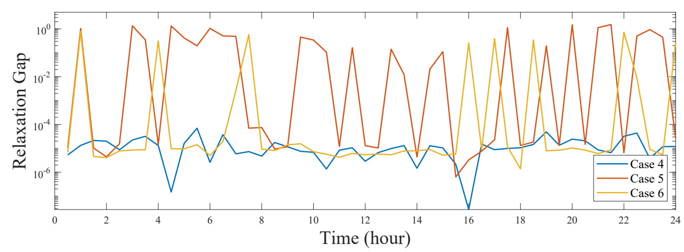

Fig. 7. Hourly gap on IEEE 13-bus for different CVR optimization methods.

V. Validation of Voltage Error Issues

Despite employing increasingly accurate OPF algorithms, noticeable voltage errors still persist. While SOCP formulations do not guarantee exact solutions in unbalanced systems [16], significant deviations can occur even when the relaxation gap is small. For instance, as illustrated in Fig. 7, the solution of Case 6 is exact between 4:00–6:00 and 8:00–15:00; nevertheless, the voltage MAPE remains as high as 1.2%. This observation suggests that the errors are not primarily caused by the inexactness of the relaxation. Instead, we attribute these discrepancies mainly to the limited accuracy of the static ZIP model used in the OPF formulation. To rigorously evaluate the impact of uncertain residential load parameters on OPF accuracy, two distinct load sets were implemented on the IEEE 123-bus feeder. The first set consists of static ZIP loads with fully specified parameters consistent with those assumed in the OPF model, whereas the second replaces these static loads with detailed residential load models configured using the same stochastic residential load setup described in Section III-A. The feeder topology and component data follow the standard IEEE configuration.

To ensure a consistent comparison of error sensitivity with respect to load size, the OPF was conducted under conditions where the residential load and the static ZIP load were of

979-8-3315-8138-1

TABLE III
COMPARISON OF OPF RESULTS UNDER STATIC ZIP AND RESIDENTIAL LOAD MODELS.

Load type	Case	MAPE (%)	Relaxation gap
Static ZIP load	3	0.8398	–
	4	0.8086	1.26e-05
	5	0.7363	0.6257
	6	0.7868	3.71e-06
Residential load	3	11.90	–
	4	11.92	2.42e-05
	5	12.05	0.1029
	6	12.04	3.17e-06

nearly equal magnitude. The results are summarized in Table III. Case 6 achieved tight SOCP relaxation solutions for both types of load, as indicated by the near-zero relaxation gaps. For the static ZIP load, voltage mismatches remain relatively small, close to those reported in [17]. In contrast, the residential load produces pronounced voltage mismatches. Since the relaxation gap sizes for both types of load are comparable, the voltage errors are not caused by the gap itself.

Unlike static ZIP loads with fully specified and time-invariant parameters, detailed residential load models involve TCLs and time-varying voltage dependence. As a result, mismatches between assumed and actual load characteristics lead to pronounced voltage estimation errors, with the increased MAPE primarily driven by load parameter uncertainty. The effect is further amplified on the IEEE 123-bus feeder: its larger size and heavier loading allow local modeling errors to propagate over longer electrical paths and accumulate across many downstream buses, resulting in a higher aggregate MAPE than in the IEEE 13-bus case.

This observation motivates the adoption of adaptive load parameter tracking in practical CVR implementations. From an implementation perspective, online load parameter tracking is computationally feasible, as it relies on the same nodal voltage and power measurements already used in CVR operation. The required update rate is governed by the time scale of residential load evolution, which typically occurs over minutes. As a result, adaptive parameter updates can be integrated into online CVR control without imposing significant communication burden.

VI. CONCLUSION

Using closed-loop MATLAB–GridLAB-D co-simulation on the IEEE 13- and 123-bus feeders, this paper benchmarks four CVR-oriented OPF formulations with increasing fidelity. Higher-fidelity unbalanced models with phase coupling reduce the mismatch between optimized voltage setpoints and simulated responses, but residual errors persist. These errors are dominated by load-model mismatch, as fixed ZIP coefficients cannot capture time-varying load composition or TCL dynamics. As a result, voltage overestimation reduces achievable CVR savings, whereas voltage underestimation increases undervoltage risk and constrains reliable deployment.

Practical CVR therefore requires real-time estimation of voltage-dependent load parameters. Future work will focus on online parameter identification and robust CVR formulations under load-parameter uncertainty, complemented by reactive power droop control for additional voltage support. We will also use the co-simulation framework to assess the impact of OPF delays on CVR performance, since OPF runtimes can become non-negligible for large-scale feeders.

REFERENCES

[1] S. Karamdel, X. Liang, and S. O. Faried, "A Novel Stochastic Volt/VAR/Pressure Optimization-Based Conservation Voltage Reduction Technique in Integrated Electricity and Natural Gas Systems With PV Smart Inverters," *IEEE Trans. on Ind. Applicat.*, vol. 61, no. 2, pp. 2271–2286, Mar. 2025.

[2] Q. Zhang, K. Dehghanpour, and Z. Wang, "Distributed CVR in Unbalanced Distribution Systems With PV Penetration," *IEEE Trans. Smart Grid*, vol. 10, no. 5, pp. 5308–5319, Sep. 2019.

[3] X. Sun, J. Qiu, Y. Tao, Y. Ma, and J. Zhao, "A Multi-Mode Data-Driven Volt/Var Control Strategy With Conservation Voltage Reduction in Active Distribution Networks," *IEEE Trans. Sustain. Energy*, vol. 13, no. 2, pp. 1073–1085, Apr. 2022.

[4] V. B. Pamshetti, S. Singh, A. K. Thakur, and S. P. Singh, "Multistage Coordination Volt/VAR Control With CVR in Active Distribution Network in Presence of Inverter-Based DG Units and Soft Open Points," *IEEE Trans. on Ind. Applicat.*, vol. 57, no. 3, pp. 2035–2047, May 2021.

[5] S. Paul and N. P. Padhy, "A New Real Time Energy Efficient Management of Radial Unbalance Distribution Networks Through Integration of Load Shedding and CVR," *IEEE Trans. Power Delivery*, vol. 37, no. 4, pp. 2571–2586, Aug. 2022.

[6] A. Bokhari, A. Alkan, R. Dogan, M. Diaz-Aguilo, F. De Leon, D. Czarkowski, Z. Zabar, L. Birenbaum, A. Noel, and R. E. Uosef, "Experimental Determination of the ZIP Coefficients for Modern Residential, Commercial, and Industrial Loads," *IEEE Trans. Power Delivery*, vol. 29, no. 3, pp. 1372–1381, Jun. 2014.

[7] Z. S. Hosseini, M. Mahoor, A. Khodaei, M. S. Hossan, W. Fan, P. Pabst, and E. A. Paaso, "Sensitivity Analyses of CVR Measurement and Verification Methodologies to Data Availability and Quality," *IEEE Access*, vol. 9, pp. 157 203–157 214, 2021.

[8] K. P. Schneider and J. C. Fuller, "Detailed end use load modeling for distribution system analysis," in *IEEE PES General Meeting*. Minneapolis, MN: IEEE, Jul. 2010, pp. 1–7.

[9] M. Farivar, Lijun Chen, and S. Low, "Equilibrium and dynamics of local voltage control in distribution systems," in *52nd IEEE Conference on Decision and Control*. Firenze: IEEE, Dec. 2013, pp. 4329–4334.

[10] M. M.-U.-T. Chowdhury, B. D. Biswas, and S. Kamalasadan, "Second-Order Cone Programming (SOCP) Model for Three Phase Optimal Power Flow (OPF) in Active Distribution Networks," *IEEE Trans. Smart Grid*, vol. 14, no. 5, pp. 3732–3743, Sep. 2023.

[11] "American National Standard for Electric Power Systems and Equipment. Voltage Ratings (60 Hertz)," ANSI C84.1, 2020.

[12] R. Singh, F. Tuffner, J. Fuller, and K. Schneider, "Effects of distributed energy resources on conservation voltage reduction (CVR)," in *IEEE PES General Meeting*. San Diego, CA: IEEE, Jul. 2011, pp. 1–7.

[13] T. D. Hardy, B. Palmintier, P. L. Top, D. Krishnamurthy, and J. C. Fuller, "HELICS: A Co-Simulation Framework for Scalable Multi-Domain Modeling and Analysis," *IEEE Access*, vol. 12, pp. 24 325–24 347, 2024.

[14] F. U. Nazir, B. C. Pal, and R. A. Jabr, "Approximate Load Models for Conic OPF Solvers," *IEEE Trans. Power Syst.*, vol. 36, no. 1, pp. 549–552, Jan. 2021.

[15] W. Price, K. Wirgau, A. Murdoch, J. Mitsche, E. Vaahedi, and M. El-Kady, "Load modeling for power flow and transient stability computer studies," *IEEE Trans. Power Syst.*, vol. 3, no. 1, pp. 180–187, Feb. 1988.

[16] L. Gan, N. Li, U. Topcu, and S. H. Low, "Exact Convex Relaxation of Optimal Power Flow in Radial Networks," *IEEE Trans. Automat. Contr.*, vol. 60, no. 1, pp. 72–87, Jan. 2015.

[17] H. Lin, F. Ui Nazir, B. C. Pal, and Y. Guo, "A Linearized Branch Flow Model Considering Line Shunts for Radial Distribution Systems and Its Application in Volt/VAr Control," *J. mod. power syst. clean energy*, vol. 11, no. 4, pp. 1191–1200, 2023.

979-8-3315-8138-1